Spin-Orbital Density Wave and a Mott Insulator in a Two-Orbital Hubbard Model on a Honeycomb Lattice

Zheng Zhu, D. N. Sheng, and Liang Fu

Phys. Rev. Lett. **123**, 087602 — Published 23 August 2019

DOI: 10.1103/PhysRevLett.123.087602

Spin/orbital density wave and Mott insulator in two-orbital Hubbard model on honeycomb lattice

Zheng Zhu,[1,2] D. N. Sheng,[2,*] and Liang Fu[1,†]

[1]*Department of Physics, Massachusetts Institute of Technology, Cambridge, MA, 02139, USA*
[2]*Department of Physics and Astronomy, California State University, Northridge, CA, 91330, USA*

(Dated: July 30, 2019)

Inspired by recent discovery of correlated insulating states in twisted bilayer graphene (TBG), we study a two-orbital Hubbard model on the honeycomb lattice with two electrons per unit cell. Based on the real-space density matrix renormalization group (DMRG) simulation, we identify a metal-insulator transition around $U_c/t = 2.5 \sim 3$. In the vicinity of U_c, we find strong spin/orbital density wave fluctuations at commensurate wavevectors, accompanied by weaker incommensurate charge density wave (CDW) fluctuations. The spin/orbital density wave fluctuations are enhanced with increasing system sizes, suggesting the possible emergence of long-range order in the two dimensional limit. At larger U, our calculations indicate a possible nonmagnetic Mott insulator phase without spin or orbital polarization. Our findings offer new insights into correlated electron phenomena in twisted bilayer graphene and other multi-orbital honeycomb materials.

Introduction.—The metal-insulator transition (MIT) driven by electron repulsion is one of the long-standing issues in condensed matter physics [1–3]. In particular, the systems with multiple orbits may harbor different exotic phases and novel phase transitions due to the interplay between orbit, spin and charge degrees of freedom.

Recently, correlated insulators were discovered at low temperature in twisted bilayer graphene (TBG) with an integer number of electrons per superlattice unit cell [4–6]. These insulating states are found near the "magic" twist angle [4, 5] or under pressure [6], where the lowest mini-band of TBG has a very narrow bandwidth. As a result of the reduced kinetic energy, the correlation effect becomes significant and most likely is the driving force for the MIT. The nature of the insulating states is now under intensive study [7–21]. A paradigmatic theoretical model for MIT is the Hubbard model and its various generalizations to include multiple orbits and extended interactions. For TBG, a two-orbital extended Hubbard model on the honeycomb lattice [7, 22] was recently derived from symmetry-adapted maximally-localized Wannier states of the low-energy bands [22, 23]. Since these low-energy bands are well separated from higher bands by a sufficiently large energy gap [24, 25], this two-orbital extended Hubbard model is a reasonable and adequate starting point for studying correlated electron phenomena in TBG [22, 26]. In this model, the two sublattices of the emergent honeycomb lattice correspond to Wannier states centered at AB and BA stacking regions, and the two orbits are associated with states from opposite valleys of graphene.

In a completely different context, the two-orbital $SU(4)$-symmetric Hubbard model on the honeycomb lattice was recently proposed for d^1 transition metal compounds with edge-sharing anion octahedra such as α-$ZrCl_3$ [27], where spin and orbital combined together describe the $j = 3/2$ quartets that emerge in the strong spin-orbit-coupling limit.

In addition to its potential relevance to real materials, it is also of fundamental importance to study the physics beyond $SU(2)$. In contrast to large-S representations of $SU(2)$, the quantum fluctuations in $SU(N)$ increase with N and thus opening new realm to explore more intriguing physics. In this work, we study the two-orbital Hubbard model with $SU(4)$ symmetry on the honeycomb lattice at quarter filling, i.e., with two fermions per unit cell. Based on large-scale density matrix renormalization group [28] (DMRG) simulations, we examine the nature of the ground state with the ratio of on-site Coulomb repulsion U and bandwidth t. We identify a MIT occurs around $U_c/t = 2.5 \sim 3$ and a nonmagnetic Mott insulator in the large U regime. Interestingly, in the vicinity of U_c, we find a small region where both spin/orbital density wave (SODW) and charge density wave (CDW) fluctuations become strong. The SODW fluctuations have commensurate wavevectors near U_c, and become enhanced when increasing system size, indicating long-range SODW order in the two dimensional (2D) limit. In contrast, the CDW fluctuations have incommensurate wavevectors and are unstable against increasing system size. The SODW is robust against perturbations including nearest neighbor interactions or lightly doping. We do not find any sign of spin/orbital polarization in the ground state.

Our findings of the nonmagnetic Mott insulator at large U is consistent with previous studies of the $SU(4)$ Heisenberg model on honeycomb lattice [29, 30], which is the effective Hamiltonian of our Hubbard model in $U/t \to \infty$ limit. Meanwhile, our finding of the SODW near MIT at intermediate U is a new result. Our work shows that the phase diagram of $SU(4)$ Hubbard model is distinctly different from SU(2) case [31–39], where a magnetic ordered phase often appears in large U limit, a direct phase transition[33–37] or an intermediate phase[31, 32, 38, 39] are found close to the MIT. It is also distinguished from half-filled $SU(2N \geq 4)$ case, where a direct transition from semimetal to valence bond solid was identified[40, 41].

Model and Method.—We consider a $SU(4)$ symmetric two-orbital Hubbard model on the honeycomb lattice. The

model is given by

$$H = H_0 + H_{\rm int}, \tag{1}$$

$$H_0 = -t \sum_{\langle i,j\rangle\sigma} \sum_{\alpha=1,2} \left(c^\dagger_{i\sigma,\alpha} c_{j\sigma,\alpha} + h.c. \right), \tag{2}$$

$$H_{\rm int} = U \sum_i \left(\sum_{\sigma,\alpha} n_{i\sigma,\alpha} - 1 \right)^2, \tag{3}$$

where $\alpha = 1, 2$ denote two orbits. $c^\dagger_{i\sigma,\alpha}$ ($c_{i\sigma,\alpha}$) represents the electron creation (annihilation) in orbit α at the ith site with spin σ ($\sigma = \uparrow, \downarrow$). $n_{i\sigma,\alpha}$ is the electron number operator. For each orbit, the honeycomb lattice on the torus or cylinder is spanned by length vectors $\mathbf{L_x} = L_x \mathbf{e_x}$ and $\mathbf{L_y} = L_y \mathbf{e_y}$, where $\mathbf{e_x} = (1, 0)$ and $\mathbf{e_y} = (1/2, \sqrt{3}/2)$ are two primitive vectors, then the total number of sites for each orbit is $N_0 = L_x \times L_y \times 2$, where L_x and L_y represent the number of unit cells along the two primitive-vector directions. For the two-orbital system on honeycomb lattice we have the number of sites $N = 2 \times N_0$ (where 2 denotes two orbits) and the number of electrons $N_e = N_0$ for a quarter filling.

We set t as the unit of energy and consider Coulomb repulsion $U > 0$. Given the additional sublattice and orbital degrees of freedom, we mainly focus on the cylinders or torus with circumferences up to $L_y = 4$ unit cells ($2 \times L_y = 8$ lattice sites in each orbit). In the present calculations, we keep up to 8000 states with enough number of sweeps to get the converged data, the truncation error is of the order or less than 10^{-4}. We also benchmark against quantum Monte Carlo (QMC) for single orbital model[47].

Metal-Insulator Transition.—We begin with studying the expectation value of the double occupancy n_d $n_d = \frac{1}{N_0} \sum_{i=1}^{N_0} \left\langle \left[\sum_{\sigma,\alpha} n_{i\sigma,\alpha} - 1 \right]^2 \right\rangle$, which corresponds to the first order derivative of the ground-state energy and is a good measurement for the Mott transition. Figures 1 (a) and (b) show n_d versus U/t for the model Hamiltonian (1) on torus and cylinder. With the increase of U/t, n_d monotonically decreases, which eventually freezes the charge degrees of freedom. The kinks of each curve and crossing of different curves with different lattice sizes indicate the transition takes place near $U_c/t = 2.5 \sim 3$, which are independent of lattice geometries we employed. We also show $U \cdot n_d$ as a function of U/t in the insets of Fig. 1, where the peaks in the curves may characterize the transition since the derivatives of the curve show discontinuity from both sides of the maximum point.

To establish the nature of each phase, we examine the momentum distribution function $n(\mathbf{k})$, which is defined by the Fourier transformation of single particle propagator $\left\langle c^\dagger_{i\sigma} c_{j\sigma} \right\rangle$, i.e., $n(\mathbf{k}) = \frac{1}{N_0} \sum_{i,j,\sigma} \left\langle c^\dagger_{i\sigma} c_{j\sigma} \right\rangle e^{i\mathbf{k}(\mathbf{r_i} - \mathbf{r_j})}$. As shown in Figure 2 (a) and (b), $n(\mathbf{k})$ shows distinct behavior before and after the transition. For the metallic phase at $U < U_c$, there is a sudden drop near the Fermi surface [see Fig. 2 (a)], while $n(\mathbf{k})$ is near flat without any singularity in the insulating side

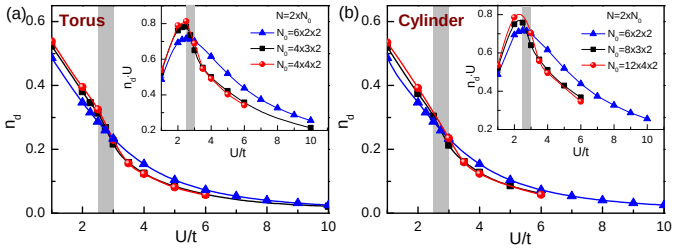

Fig. 1: The average of the double occupancy n_d as a function of U/t for torus (a) and cylinder(b) geometries. The insets show the $n_d \cdot U$ as a function of U/t. The shadow bar indicates the MIT.

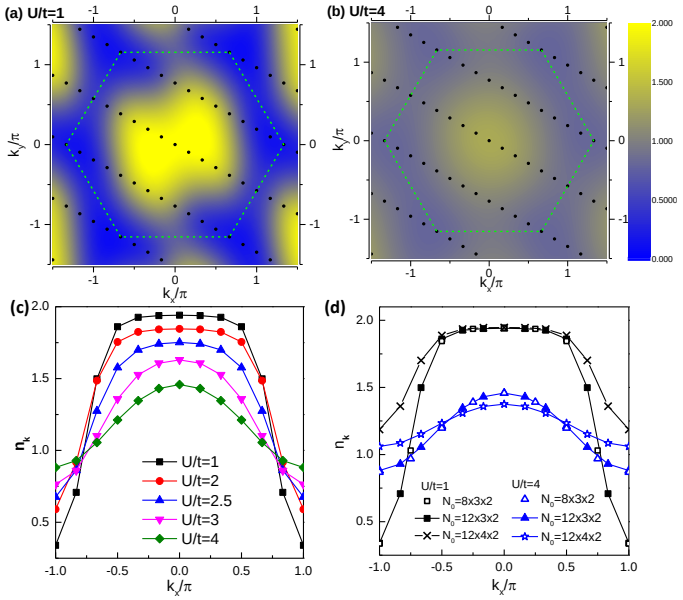

Fig. 2: The momentum distribution $n(\mathbf{k})$ for the metallic phase at $U/t = 1$ (a) and insulating phase at $U/t = 4$ (b). The black dots represent the momentum points we can access in the Brillouin zone of the finite size lattice, the contour plot is created by using triangulation interpolation. The cut of $n(\mathbf{k})$ along the line crossing Γ point for different ratios of U/t are shown in (c), where the slope of $n(\mathbf{k})$ decreases with the increase of U/t near the Fermi surface. Here, we consider the cylinders with $N_0 = 12 \times 3 \times 2$. (d) The same cut of $n(\mathbf{k})$ as (c) at $U/t = 1$ and $U/t = 4$ for different system sizes.

at $U > U_c$ [see Fig. 2 (b)]. To show the evolution of the Fermi surface with increasing U/t, we cut the $n(\mathbf{k})$ along the line crossing $\Gamma = (0, 0)$ point, as shown in Fig. 2 (c), the smooth change of the line shape indicates the continuity of this MIT, which is consistent with the behavior of n_d [see Fig 1]. In addition, We also confirm that results of $n(\mathbf{k})$ are robust against system size as illustrated in Fig. 2 (d).

Density Wave Fluctuations/Orders.— We have identified that the MIT occurs near $U_c/t = 2.5 \sim 3$. Below we examine the electronic and magnetic fluctuations and explore possible orders particularly near the MIT and in the insulating phase. Numerically the most direct evidence to explore the

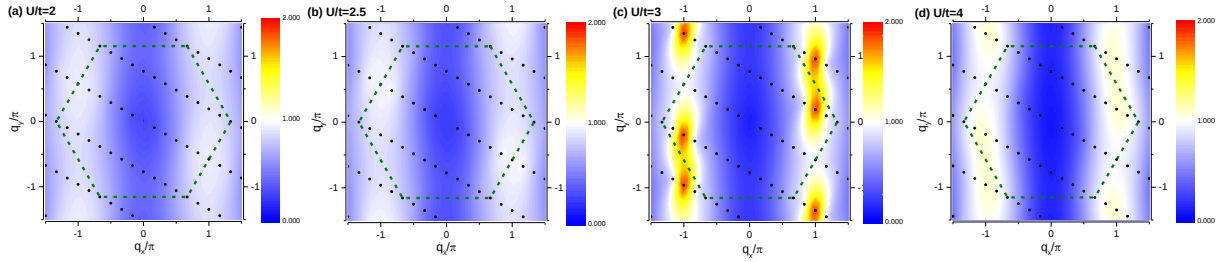

Fig. 3: The contour plot of the structure factor $N_{\mathbf{q}}$ for $L_y = 3$ cylinders at $U/t = 2$ (a) , and $U/t = 2.5$ (b) , $U/t = 3$ (c), $U/t = 4$ (d). $N_{\mathbf{q}}$ are featureless for both metallic phase (a) and insulating phase (d), while the CDW fluctuations arise in the vicinity of the MIT (c). The splitting of the CDW peaks around M point signifies the incommensurate CDW instability. Here, we consider the cylinders with $L_x = 12$ unit cells, the black dots represent the momentum points we can access in the Brillouin zone of the finite size lattice. The contour plot is created by using triangulation interpolation.

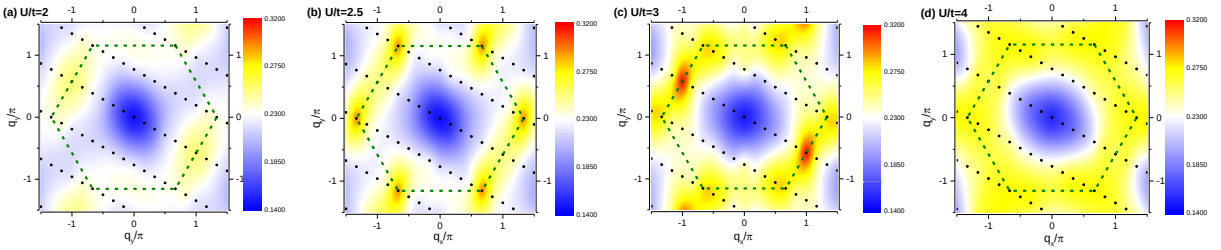

Fig. 4: The contour plot of the static spin structure factor $S_{\mathbf{q}}$ for $L_y = 3$ cylinders at $U/t = 2$ (a), $U/t = 2.5$ (b), $U/t = 3$ (c), $U/t = 4$ (d). $S_{\mathbf{q}}$ are featureless for both metallic phase (a) and insulating phase (d), while the spin/orbital density wave fluctuations arise in the vicinity of the MIT point (b-c). The peaks of $S_{\mathbf{q}}$ locate at K or M points indicating the commensurate spin/orbital density wave instability. Here, we consider the cylinders with $L_x = 12$ unit cells, the black dots represent the momentum points we can access in the Brillouin zone of the finite size lattice. The contour plot is created by using triangulation interpolation. The peaks in (c) is higher than (b), indicating the stronger fluctuations with wave vector at M points than at K points.

fluctuations or orders is to calculate the correlations and their structure factors. Here, we consider the correlations within the same sublattice, which are the same for the two sublattices. Although the systems on cylinders break translational symmetry due to the open boundaries, we find our results are robust by neglecting the boundary effects when the system size is relatively large.

We first measure the structure factor of charge density-density correlations $N_{\mathbf{q}} = \frac{1}{N_0}\sum_{i,j}\langle n_i n_j\rangle e^{i\mathbf{q}(\mathbf{r_i}-\mathbf{r_j})}$. Figures 3 shows N_q in the metallic phase, insulating phase as well as around the vicinity of the MIT. The black dots indicate the data points in the contour plot for finite size system with $L_x = 12$ and $L_y = 3$. Here we have substracted the peak at $q = 0$, which is trivially induced by the uniform charge background. Fig. 3 (a) and (d) show that there are no significant peaks in $N_{\mathbf{q}}$ deep inside both the metallic phase at $U < U_C$ and insulating phase at $U > U_C$, while near the transition point, $N_{\mathbf{q}}$ displays strong charge density wave (CDW) fluctuations, as shown in Fig. 3 (c). When $U/t = 3$, the peaks in N_q locate at available momenta nearby $\mathbf{M}$ points, implying the incommensurate nature of such CDW fluctuations. We also check the finite size effect by studying wider cylinder with $L_y = 4$, as shown in the Fig. 5 (a). N_q also displays significant peaks around $\mathbf{M}$ but with different wave vectors, which is consistent with the fact that the wave vectors of the incommensurate CDW fluctuations depend on the system geometry. Meanwhile, we also notice that the intensity of N_q is weakened with increasing the width of cylinders, as shown in Fig. 3 (c) and Fig. 5 (a), which suggests the CDW fluctuations are not strong enough to form CDW order towards 2D limit.

In the spin channel, we study the static spin structure factor to detect the magnetic fluctuations, which is defined as the Fourier transformation of spin-spin correlations, i.e., $S_{\mathbf{q}} = \frac{1}{N_0}\sum_{i,j}\left\langle S_i^z S_j^z\right\rangle e^{i\mathbf{q}(\mathbf{r_i}-\mathbf{r_j})}$, where $S_i^a \equiv \sum_\alpha\sum_{\sigma\sigma'} c^\dagger_{i\sigma,\alpha} s^a_{\sigma\sigma'} c_{i\sigma',\alpha}$ is the spin operator on site i. Due to the $SU(4)$ symmetry of the Hubbard model, the orbital and spin correlations are identical. Figures 4 show the spin/orbital structure factor $S_{\mathbf{q}}$ for different values of U/t for the same $L_y = 3$ systems with $L_x = 12$. Both the metallic phase at $U < U_C$ [see Fig. 4 (a)] and the insulating phase at $U > U_C$ [see Fig. 4 (d)] exhibit the absence of magnetic fluctuations or orders. While near U_c, $S_{\mathbf{q}}$ displays strong SODW fluctuations, as shown in Fig. 4 (b) and Fig. 4 (c). Interestingly, the SODW fluctuations display competing wave vectors at commensurate momentum $\mathbf{K}$ or $\mathbf{M}$, which depend on the values of ratio between Coulomb interaction and bandwidth. When

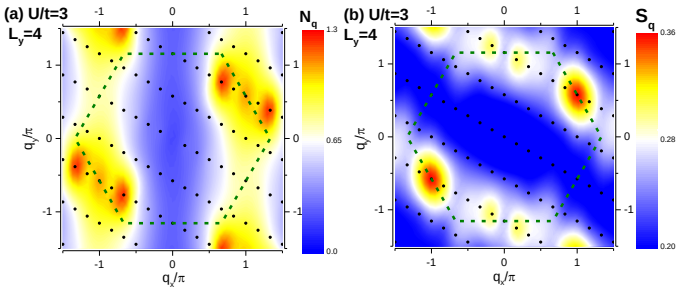

Fig. 5: The structure factor $N_{\mathbf{q}}$ (a) and $S_{\mathbf{q}}$ (b) for $L_y = 4$ systems at $U/t = 3$. Here, we consider the cylinders with $L_x = 12$, the black dots represent the momentum points we can access in the Brillouin zone of finite size lattice system. The contour plot is created by using triangulation interpolation.

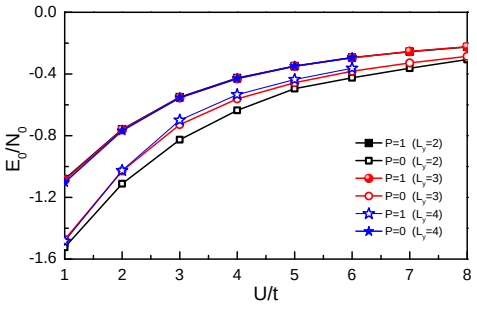

Fig. 6: The ground state energy E_0 per site as a function of U/t for both unpolarized $P = 0$ and polarized $P = 1$ sectors. Here, we consider the systems with $L_x = 12$ and different L_y.

$U/t = 2.5$ [see Fig. 4(c)], there are peaks located at $\mathbf{K}^+ = (4\pi/3, 0)$ and $\mathbf{K}^- = (2\pi/3, 2\pi/\sqrt{3})$ points in the Brillouin zone. However, further increasing the ratio to $U/t = 3$ [see Fig. 4(d)], the peaks of $S(q)$ near $\mathbf{K}^{\pm}$ become broader while much sharper peaks arise at $M = (\pm\pi, \mp\pi/\sqrt{3})$ points, indicating the SODW fluctuations with wave vector $\mathbf{M}$ are more dominant than the ones with wave vector $\mathbf{K}$ near U_c This can be seen more clearly by increasing the cylinder width towards 2D, as shown in the Fig. 5 (b) for S_q on $L_y = 4$ cylinders, where the SODW fluctuations display significant peaks around $\mathbf{M}$. In addition, the intensity of S_q is also enhanced with increasing the system size [see Fig. 4 (c) and Fig. 5 (b)], indicating the possible existence of SODW order in 2D.

Orbital Polarizations.—We have identified strong charge and spin/orbital dentity wave fluctuations or orders near the quantum phase transition, while the structure factors indicate the featureless nonmagnetic insulating state at $U > U_c$ [see Fig. 3(d) and Fig. 4(d)]. Below, we examine polarization in the spin/orbital channel. To check the possibility of orbital polarizations of the Hamiltonian [see Eq. (1)] at a quarter filling, we define $P = |N_1 - N_2|/N_0$, where N_α ($\alpha = 1, 2$) represent the total electron number in orbit α, and then we compare the ground-state energies of the unpolarized sector with equal number of electrons in two orbits ($P = 0$) and the orbital polarized sector with all electrons in one orbit ($P = 1$). As shown in the Fig. 6 for different L_y systems, $P = 0$ sector always has lower energy than $P = 1$ sector, which is independent of the system sizes, implying the absence of the fully orbital polarization for the ground states. Due to the $SU(4)$ symmetry, this result also implies that the ground state is not fully spin-polarized. This conclusion is consistent with the absence of enhancement in the $\mathbf{q} = 0$ spin structure factor.

Discussion and Summary.—We now discuss the relevance of our work to real materials. Recently, the two-orbital $SU(4)$ Hubbard model on the honeycomb lattice at quarter filling has been proposed as a realistic model for α-$ZrCl_3$ and metal organic frameworks with tricoordinated lattices [27]. It may be possible to tune the ratio U/t by pressure and to search for spin/orbital density wave and Mott insulator states.

For TBG, the microscopic two-orbital Hamiltonian derived from band structure calculations and Coulomb interactions projected to low-energy bands has more terms than the simplest two-orbital Hubbard model studied here. It includes single-particle hoppings beyond nearest neighbors[9], extended density and exchange interactions beyond on-site U, pair hoppings [23, 42], and the effect of other Moiré bands may be important [43–45]. These additional terms can stabilize SODW[46] or lead to new phases beyond the density wave and Mott insulator states. For example, Ref.[21] found a orbital-polarized state at quarter filling induced by pair hopping, when kinetic energy is set to zero. The fully understanding the physics in TBG requires a more comprehensive study of the microscopic Hamiltonian. Nonetheless, the current two-orbital Hubbard model with the nearest-neighbor hopping and on-site repulsion may be served as a starting and reference point to study correlated electron physics of TBG.

In summary, based on DMRG simulations of the two-orbital Hubbard model on honeycomb lattice, we identify a MIT near $U_c/t \approx 2.5 \sim 3$ accompanied by commensurate SODW orders and incommensurate CDW fluctuations, and find a nonmagnetic Mott insulator without orbital polarization at $U > U_c$. Our results enrich the Mott physics near MIT, where a SODW emerges as an intermediate phase. We also find the SODW is robust against lightly doping and the weak nearest neighbor (NN) interactions[47, 48]. In addition, we have also checked that there is no indication of any density waves at 1/8 filling[47] , which corresponds to one electron per unit cell. Our findings can be tested experimentally in TBG, where applying pressure can drive the system across MIT and deep into the Mott insulator [6].

We thank A. Vishwanath, S. K. Jian and Masahiko Yamada for helpful discussions. This research was carried out through the support of the David and Lucile Packard foundation (Z.Z., L.F.). This work carried out at CSUN was supported by the U.S. Department of Energy (DOE), Office of Basic Energy Sciences under Grant No. DEFG02-06ER46305 (Z.Z., D.N.S.). D.N.S. also acknowledges support from the DOE, the Office of Basic Energy Sciences, Division of Materials Sciences and Engineering, under Contract No. DE-

AC02-76SF00515 through SLAC National Accelerator Laboratory for the development of numerical methods extensively applied to this project.

* donna.sheng1@csun.edu
† liangfu@mit.edu

[1] N. F. Mott, *The Basis of the Electron Theory of Metals, with Special Reference to the Transition Metals*, Proc. Phys. Soc. London, Ser. A **62**, 416 (1949); N. F. Mott, *On the transition to metallic conduction in semiconductors*, Can. J. Phys. **34**, 1356(1956); N. F. Mott, *The transition to the metallic state*, Philos. Mag. **6**, 287(1961).

[2] N. F. Mott, *Metal-Insulator Transitions* (Taylor and Francis,London, UK, 1990).

[3] M. Imada,A. Fujimori, andY. Tokura, *Metal-insulator transitions*, Rev. Mod. Phys. **70**, 1039(1998) and references therein.

[4] Y. Cao, V. Fatemi, S. Fang, K. Watanabe, T. Taniguchi, E. Kaxiras, and P. Jarillo-Herrero, *Unconventional superconductivity in magic-angle graphene superlattices*, Nature **556**, 43 (2018).

[5] Y. Cao, V. Fatemi, A. Demir, S. Fang, S. L. Tomarken, J. Y. Luo, J. D. Sanchez-Yamagishi, K. Watanabe, T. Taniguchi, E. Kaxiras, R. C. Ashoori, and P. Jarillo-Herrero, *Correlated insulator behaviour at half-filling in magic-angle graphene superlattices*, Nature **556**, 80 (2018).

[6] Matthew Yankowitz, Shaowen Chen, Hryhoriy Polshyn, K. Watanabe, T. Taniguchi, David Graf, Andrea F. Young, Cory R. Dean, *Tuning superconductivity in twisted bilayer graphene*, arXiv:1808.07865 (2018).

[7] N. F. Q. Yuan and L. Fu, *Model for the metal-insulator transition in graphene superlattices and beyond*, Phys. Rev. B **98**, 045103 (2018).

[8] C. Xu and L. Balents, *Topological Superconductivity in Twisted Multilayer Graphene*, Phys. Rev. Lett. **121**, 087001 (2018).

[9] H. C. Po, L. Zou, A. Vishwanath, T. Senthil, *Origin of Mott Insulating Behavior and Superconductivity in Twisted Bilayer Graphene*, Phys. Rev. X **8**, 031089 (2018).

[10] Hiroki Isobe, Noah F. Q. Yuan, Liang Fu, *Unconventional Superconductivity and Density Waves in Twisted Bilayer Graphene*, Phys. Rev. X **8**, 041041 (2018).

[11] Y.-Z. You and A. Vishwanath, *Superconductivity from Valley Fluctuations and Approximate SO(4) Symmetry in a Weak Coupling Theory of Twisted Bilayer Graphene*, arXiv:1805.06867.

[12] Cheng-Cheng Liu, Li-Da Zhang, Wei-Qiang Chen, and Fan Yang, *Chiral Spin Density Wave and Superconductivity in the Magic-Angle-Twisted Bilayer Graphene*, Phys. Rev. Lett. **121**, 217001(2018).

[13] J. F. Dodaro, S. A. Kivelson, Y. Schattner, X.-Q. Sun, and C. Wang, *Phases of a phenomenological model of twisted bilayer graphene*, Phys. Rev. B **98**, 075154 (2018).

[14] Guo-Yi Zhu, Tao Xiang, Guang-Ming Zhang, *Inter-valley spiral order in the Mott insulating state of a heterostructure of trilayer graphene-boron nitride*,Science Bulletin **63** 1087-1091(2018).

[15] V. Yu. Irkhin, Yu. N. Skryabin,*Dirac points, spinons and spin liquid in twisted bilayer graphene*, JETP Letters **107**, 651-654 (2018).

[16] Louk Rademaker, Paula Mellado, *Charge-transfer insulation in twisted bilayer graphene*, arXiv:1805.05294(2018).

[17] J.M. Pizarro, M.J. Calderón, E. Bascones, *The nature of correlations in the insulating states of twisted bilayer graphene*,arXiv:1805.07303.

[18] M. Ochi, M. Koshino, K. Kuroki, *Possible correlated insulating states in magic-angle twisted bilayer graphene under strongly competing interactions*,Phys. Rev. B **98**, 081102(R) (2018).

[19] Xiao Yan Xu, K. T. Law, and Patrick A. Lee, *Kekulé valence bond order in an extended Hubbard model on the honeycomb lattice with possible applications to twisted bilayer graphene*, Phys. Rev. B **98**, 121406(R) (2018).

[20] J. W. F. Venderbos, R. M. Fernandes, *Correlations and electronic order in a two-orbital honeycomb lattice model for twisted bilayer graphene*, arXiv:1808.10416.

[21] Jian Kang, Oskar Vafek, *Strong coupling phases of partially filled twisted bilayer graphene narrow bands*, arXiv:1810.08642.

[22] M. Koshino, N. F. Q. Yuan, T. Koretsune, M. Ochi, K. Kuroki, and L. Fu, *Maximally Localized Wannier Orbitals and the Extended Hubbard Model for Twisted Bilayer Graphen*, Phys. Rev. X **8**, 031087 (2018).

[23] Jian Kang and Oskar Vafek, *Symmetry, Maximally Localized Wannier States, and a Low-Energy Model for Twisted Bilayer Graphene Narrow Bands*, Phys. Rev. X **8**, 031088 (2018).

[24] Y. Cao, J. Y. Luo, V. Fatemi, S. Fang, J. D. SanchezYamagishi, K. Watanabe, T. Taniguchi, E. Kaxiras, and P. Jarillo-Herrero, *Superlattice-Induced Insulating States and Valley-Protected Orbits in Twisted Bilayer Graphene*, Phys. Rev. Lett. **117**, 116804 (2016).

[25] N. N. T. Nam and M. Koshino, *Lattice relaxation and energy band modulation in twisted bilayer graphene*, Phys. Rev. B **96**, 075311 (2017).

[26] N. F. Q. Yuan and L. Fu, to appear.

[27] Masahiko G. Yamada, Masaki Oshikawa, and George Jackeli, *Emergent $SU(4)$ Symmetry in α-$ZrCl_3$ and Crystalline Spin-Orbital Liquids*, Phys. Rev. Lett. **121**, 097201 (2018).

[28] S. R. White, Density matrix formulation for quantum renormalization groups, Phys. Rev. Lett. **69**, 2863 (1992).

[29] Philippe Corboz, Miklós Lajkó, Andreas M. Läuchli, Karlo Penc, and Frédéric Mila, *Spin-Orbital Quantum Liquid on the Honeycomb Lattice*, Phys. Rev. X **2**, 041013 (2012).

[30] Miklós Lajkó and Karlo Penc, *Tetramerization in a SU(4) Heisenberg model on the honeycomb lattice*, Phys. Rev. B **87**, 224428 (2013).

[31] Z. Y. Meng, T. C. Lang, S. Wessel, F. F. Assaad , A. Muramatsu, *Quantum spin liquid emerging in two-dimensional correlated Dirac fermions*, Nature **464**, 847 (2010).

[32] Q. Chen, G.H. Booth, S. Sharma, G. Knizia, and G.K.-L. Chan, Intermediate and Spin-Liquid Phase of the Half-Filled Honeycomb Hubbard Model, Phys. Rev. B 89, 165134 (2014).

[33] Sandro Sorella, Yuichi Otsuka, Seiji Yunoki, *Absence of a Spin Liquid Phase in the Hubbard Model on the Honeycomb Lattice*, Sci. Rep. **2**, 992 (2012).

[34] F. F. Assaad and I. F. Herbut, *Pinning the Order: The Nature of Quantum Criticality in the Hubbard Model on Honeycomb Lattice*, Phys. Rev. X **3**, 031010 (2013).

[35] S. R. Hassan and D. Sénéchal, *Absence of Spin Liquid in Nonfrustrated Correlated Systems*, Phys. Rev. Lett. **110**, 096402 (2013).

[36] F. Parisen Toldin, M. Hohenadler, F.F. Assaad, and I.F. Herbut, *Fermionic Quantum Criticality in Honeycomb and π-flux Hubbard Models: Finite-Size Scaling of Renormalization-Group-Invariant Observables from Quantum Monte Carlo*, Phys. Rev. B **91**, 165108 (2015).

[37] Yuichi Otsuka, Seiji Yunoki, and Sandro Sorella, *Universal Quantum Criticality in the Metal-Insulator Transition of Two-Dimensional Interacting Dirac Electrons*, Phys. Rev. X **6**,

011029 (2016).

[38] Tomonori Shirakawa, Takami Tohyama, Jure Kokalj, Sigetoshi Sota, and Seiji Yunoki, *Ground-state phase diagram of the triangular lattice Hubbard model by the density-matrix renormalization group method*, Phys. Rev. B **96**, 205130 (2017).

[39] Aaron Szasz, Johannes Motruk, Michael P. Zaletel, Joel E. Moore, *Observation of a chiral spin liquid phase of the Hubbard model on the triangular lattice: a density matrix renormalization group study*, arXiv:1808.00463.

[40] Zhichao Zhou, Da Wang, Zi Yang Meng, Yu Wang, and Congjun Wu, *Mott insulating states and quantum phase transitions of correlated SU(2N) Dirac fermions*, Phys. Rev. B **93**, 245157 (2016).

[41] Zi-Xiang Li and Hong Yao, *Sign-Problem-Free Fermionic Quantum Monte Carlo: Developments and Applications*, Annu. Rev. Condens. Matter Phys. **10** 337 (2019), and the references therein. Zi-Xiang Li, Yi-Fan Jiang, Shao-Kai Jian, and Hong Yao, *Fermion-induced quantum critical points*, Nat Commun 8 314 (2017).

[42] Francisco Guinea and Niels R. Walet, *Electrostatic effects, band distortions, and superconductivity in twisted graphene bilayers*, Proceedings of the National Academy of Sciences , 115 (52) 13174 (2018)

[43] Kasra Hejazi, Chunxiao Liu, Hassan Shapourian, Xiao Chen, Leon Balents, *Multiple topological transitions in twisted bilayer graphene near the first magic angle*, arXiv:1808.01568

[44] Zhida Song, Zhijun Wang, Wujun Shi, Gang Li, Chen Fang, B. Andrei Bernevig, *All "Magic Angles" Are "Stable" Topological*, arXiv:1807.10676.

[45] Hoi Chun Po, Liujun Zou, T. Senthil, Ashvin Vishwanath, *Faithful Tight-binding Models and Fragile Topology of Magic-angle Bilayer Graphene*, arXiv:1808.02482.

[46] Constantin Schrade, Liang Fu, to be published.

[47] See supplementary materials.

[48] T. O. Wehling, E. Şaşıoğlu, C. Friedrich, A. I. Lichtenstein, M. I. Katsnelson, and S. Blügel, *Strength of Effective Coulomb Interactions in Graphene and Graphite*, Phys. Rev. Lett. **106**, 236805 (2011).